Using a network of 2D video disdrometers for external radar calibration of NASA's S-band polarimetric radar

V. N. Bringi[1], M. Thurai[1], W. A. Petersen[2], and P. N. Gatlin[3]

[1]Colorado State Univ., Fort Collins, Colorado
[2] NASA/GSFC, Wallops, Virginia
[3] NASA/MSFC, Huntsville, Alabama

1. Introduction

A fundamental requirement of weather radars is accurate calibration of the absolute reflectivity, the oft quoted figure being within ± 1dB, but for quantitative application such as hourly rain accumulation (especially for extreme events), a smaller uncertainty of ±0.5dB can be regarded as a goal. To a large extent, maintenance of an initial calibration state can be realized using either on-line or off-line procedures, e.g., continuous monitoring of transmit power, receiver calibration using test signal generators, standard noise source injection, etc (e.g., Cavalli 1998; Free et al 2005). When combined with modern high quality test equipment together with advances in the performance of analog front ends, digital IF receivers and programmable signal processors, the overall relative stability of the radar system can be maintained at a very high level (e.g., Cavalli 1998; Darlington et al 200x), the level of uncertainty so realized being much less than that due to the natural spatio-temporal variability of the precipitation. Attaining the objective of absolute accuracy is more difficult and relies on standard external targets/sources such as, for example, metal spheres, solar flux, passive or active calibrators, etc. However, it is generally accepted that the standard methods cannot achieve uncertainty levels of ±0.5 dB (through error budget considerations). Other methods such as self-consistency (Goddard et al., 1994) use polarimetric data from rain [Z_h, Z_{dr}, K_{dp}] to calibrate the system offsets in Z_h but uncertainties in the assumed mean drop axis ratio versus D relation as well as dependence on filtering/thresholding of the polarimetric data precludes achieving the elusive figure of ±0.5 dB.

In this paper, we consider the use a network of closely-spaced 2D-video disdrometers (2DVD) to calibrate the absolute Z_h measured by NASA's S-band polarimetric radar (NPOL). This differs from earlier use of single disdrometers for absolute calibration of profilers or scanning weather radars. The use of multi-disdrometer network has the obvious advantage of greatly increasing the sample size thereby enabling more precise estimation of the uncertainty of the calibration offset. In addition, the calibration is based on rainfall which constitutes a volume-filled target (preferably uniform rain).

During the MC3E campaign (Petersen and Jensen, 2012) in Oklahoma, the NPOL radar performed repeated PPI scans over a network of six 2DVD sites, located 20 to 30 km from the radar with a repeat cycle times of approximately 40 seconds. One 4-hour event is considered here in order to demonstrate our calibration procedure, not only for Z_h but also for Z_{dr}. To validate the

calibration offsets, we compare radar-based rainfall rates and (more importantly) rainfall accumulations with those from the six 2DVDs. A second event is considered for further verification.

2. NPOL scans and 2DVD data

The MC3E field experiment took place in central Oklahoma from April to June 2011 in the region of the Southern Great Plains, where an extensive array of both airborne and ground-based instrumentation was deployed. More information can be found in Petersen and Jensen (2012). The overarching goals of the field effort were to provide a complete three-dimensional characterization of precipitation microphysics in the context of improving the reliability of GPM precipitation retrievals over land, and to advance understanding of the primary physical components that form the basis for models that simulate convection and clouds.

Fig. 1a shows the map of the campaign location. The white triangle depicts the area within which the 2DVDs were sited, and the area where the repeated PPI scans were performed. Fig. 1b shows one such PPI scan together with the locations of the six 2DVD units shown as black crosses. The spacing of the six instruments enables us to determine the 'point' spatial correlation function of the calculated radar reflectivity which in turn can be compared with radar-based estimation of the 'pixel-based' correlation function. Additionally, the 40 sec repeat time of the PPI scans may be considered as being lower than the decorrelation time for the radar reflectivity field (Thurai et al., 2012), at least in the events considered herein.

The precipitation event considered here was a mesoscale convective complex which occurred on 11 May 2011. Fig. 1c shows the NEXRAD national mosaic reflectivity image for this event at 19:38 UTC. However, the storm area captured by the NPOL scans reflected short periods of convection with a longer duration stratiform rain component that exhibited relatively modest reflectivity (< 40 dBZ).

(a)

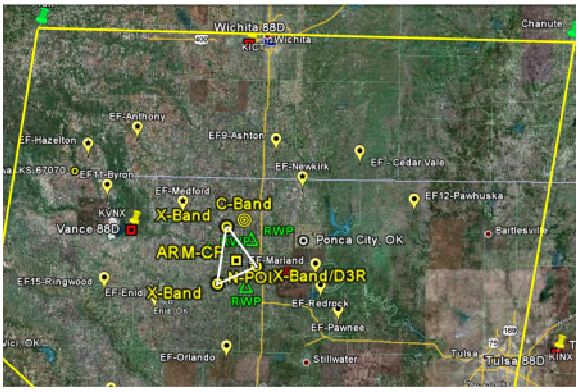

(b)

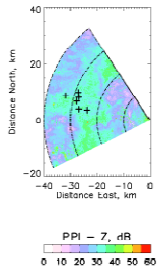

(c)

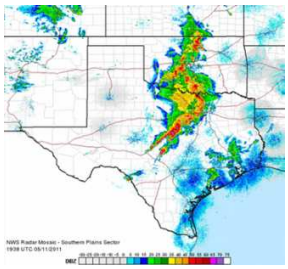

Figure 1. (a) Map of MC3E study domain. (b) A PPI scan performed by NPOL over the 2DVDs (crosses). (c) NEXRAD mosaic of reflectivity on 11 May 2011.

a. Radar data processing

The initial processing of radar data comprised several standard procedures, as follows:

- For each recorded range profile, the meteorological / non-meteorological echo separation is made, primarily using the standard deviation of the

differential propagation phase, Φ_{dp} and the copolar correlation coefficient, ρ_{hv}; this is followed by the use of the so-called hail detection ratio (often abbreviated as HDR and defined in Aydin et al., 1986, but originally proposed by Hall et al 1984 and Bringi et al. 1984) to identify locations of hail or melting graupel.

- The Φ_{dp} range profile is FIR (finite impulse response) filtered using the technique described in Hubbert and Bringi (1995) to determine the specific differential propagation phase (K_{dp}); this method also has the advantage of quantifying and removing any contribution from back-scatter differential phase.

- Additionally, because the measured Z_{dr} is generally "noisy", the FIR filtering (i.e. the same technique used for Φ_{dp} filtering) is also used to filter out the high frequency gate-to-gate fluctuations.

- An attenuation-correction scheme based on Ryzhkov et al. (2005) is employed in order to correct for small attenuation and differential attenuation at S-band. The coefficients relating attenuation and differential attenuation to Φ_{dp} are applicable to summer-time Oklahoma rain storms. In the event/s analyzed here, the attenuation correction was almost negligible.

- For initial calibration assessment, consistency checks are used to determine Z_h and Z_{dr} calibrations from the 'two-dimensional histograms' representing the contoured frequency of occurrence plots for K_{dp} versus Z_h, and Z_{dr} versus Z_h, following the procedure described in Bringi et al. (2006). The calculations based on the aforementioned 1-minute DSDs are superimposed to assess the deviation from the initial calibration offsets, if any.

(b) Comparison with DSD based calculations

The Z_h extracted from each PPI scan over the six 2DVD locations (and neighboring 8 pixels: 2 adjacent beams and 2 adjacent range gates) are shown as time series in Fig. 2, represented by blue crosses (indicating data from all pixels in each sweep). The six panels correspond to the six 2DVDs, denoted by SN25, SN35, SN36, SN37, SN38, and SN47. Superimposed on the plots are the 2DVD data based scattering calculations, shown in red. The scattering (T-matrix) calculations, based on 1-minute DSDs, were made assuming our reference drop shapes (Thurai et al., 2007) as well as the standard Gaussian distribution for drop canting angle distributions (Huang et al., 2008). The events considered here are not severe, nor intense, which would require more detailed calculations using the scattering matrix for each individual drop shape and orientation (as was done for example in Thurai et al. (2009) for an intense event). Note also that the 2DVD based calculations have been smoothed over 3 minutes using a uniformly-weighted moving average (three 1-minute samples).

The corresponding comparisons for Z_{dr} are shown in Fig. 3. As in the case of the reflectivity comparisons in Fig. 2, the differential reflectivity comparisons also show reasonably good agreement.

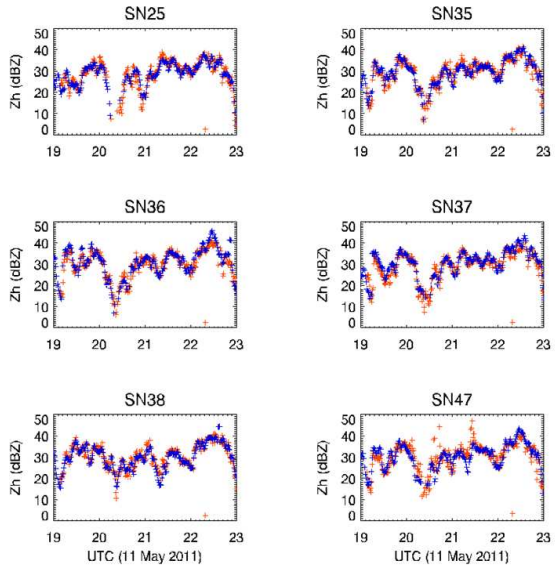

Figure 2. Z_h comparisons between N-pol data (blue crosses), and 2DVD data based estimates using 1-minute DSDs in red for the six 2DVDs deployed for the MC3E event on 11 May 2011.

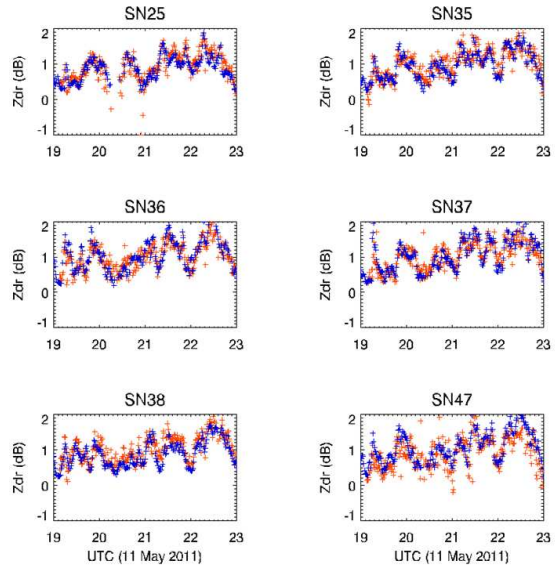

Figure 3. Same as Fig. 2 but for Z_{dr}

3. Quantitative comparisons

To make quantitative comparisons, the NPOL data needed to be interpolated - in the time domain - to the time grid of the 2DVD data (every 1-minute). In our case, linear interpolation was found to be sufficient rather than the more elaborate spline interpolation, both for Z_h and Z_{dr}. The comparisons so derived (our final results, after applying the estimated offsets) for the four hour period and for the six instruments are shown in Fig. 4 for Z_h. Each of the six panels is as follows:

The top left panel (a) shows the scatterplot of Z_h from NPOL radar (time interpolated) versus the 2DVD data-based Z_h. Comparisons from all six units are shown, with different colors representing the six different instruments. The dashed line represents the [1:1] line.

The top right panel (b) shows the comparisons for only five units; the sixth unit (SN47) was located very near a tall tower and the corresponding NPOL reflectivity may have been clutter-contaminated, and hence this was eliminated from further comparisons.

The middle left panel (c) compares the relative frequency histograms (PDF) of Z_h determined from NPOL and 2DVDs, corresponding to panel (b). The agreement is very close in terms of the mode, width and the shape of the distribution including the skewness.

For determining the calibration offsets, we further choose only the moderate reflectivity values, as shown in panel (d) which shows the scatterplot for $25 < Z_h < 35$ dBZ. This is to emphasize stratiform rain and to avoid strong reflectivity gradients.

Panel (e) represents the PDF of the differences in Z_h, given by $\Delta Z = Z_h(\text{NPOL}) - Z_h(\text{2DVD})$ determined from the points in

panel (d). The offset applied to the NPOL Z_h is shown on top of this panel (-0.8 dB).

Panel (f) is a zoomed-in version of the same histogram as in panel (e). Also shown is the fitted Gaussian curve in red, which (somewhat unexpectedly) is a very good fit to the PDF of ΔZ. The curve is almost centered at $\Delta Z = 0$. The standard deviation is 1.56 dB.

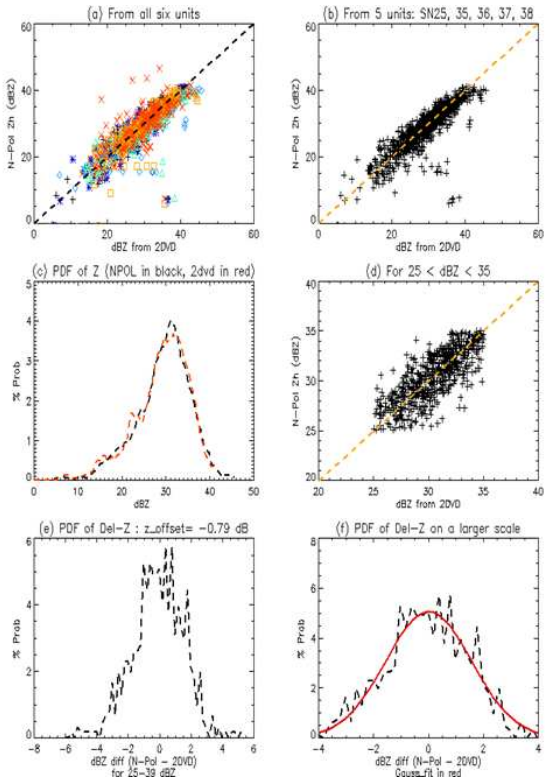

Figure 4. Comparison of Z_h from NPOL and 2DVDs (see text for explanation).

The corresponding set of panels for Z_{dr} is shown in Fig. 5. The applied offset for Z_{dr} was -0.09 dB and once again the fitted Gaussian curve seems to be a close fit to the PDF of ΔZ_{dr}, with the peak being positioned very close to zero. The standard deviation of the fitted curve was found to be 0.19 dB.

From Fig. 4 and 5, the calibration offsets of -0.8 dB and -0.09 dB applied to NPOL Z_h and Z_{dr}, respectively, appear to be accurate, since the fitted Gaussian curves for both cases are centered close to zero. The fact that the PDFs can be represented by Gaussian fit also implies that the 95% confidence interval for the mean offset can be determined.

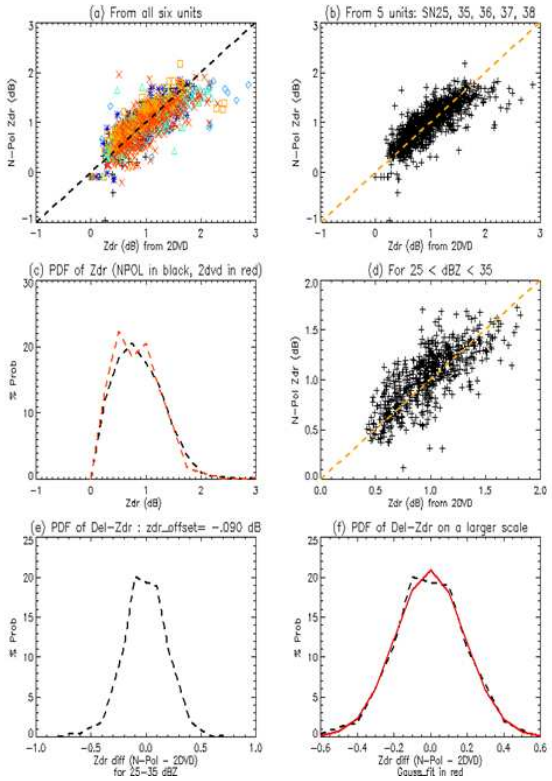

Figure 5. Comparison of Z_{dr} from NPOL and 2DVDs (see text for explanation).

The finite standard deviation of ΔZ arises partly from the fact that the radar measurements are from a relatively large volume in space at heights of around 600-700 m above ground level (corresponding to 25-32 km range and 1.3 deg elevation of the PPI scans) whilst the 2DVD-based calculations correspond to point

measurements, albeit integrated over 1 minute and smoothed over 3 minutes. Thus, some portion of the scatter in Z_h between 2DVD and radar measurements is due to the significantly different measurement scales, which is referred to as 'point-to-area variance' and needs to be accounted for in order to ensure the Z_h and Z_{dr} offsets are in fact attributable to the radar calibration. The point-to-area variance can be estimated from the spatial correlation using an approach analogous to radar-gage comparisons (error variance separation) given in Ciach and Krajewski (1999). The spatial correlation of Z_h for the 11th May event was determined in a manner similar to that given in Bringi et al. (2013, paper from this conference), which in turn was used to determine the corresponding variance reduction factor using the approach similar to Habib and Krajewski (2002). The contribution of the point-to-area variance to our observed standard deviation of ΔZ (1.56 dB as mentioned earlier) was found to be around 10%, and with a sample number of 610, we estimate the 95% confidence interval to be ±0.12 dB for our estimated calibration offset for Z_h of -0.8 dB. For Z_{dr}, the point-to-area variance was also found to be low compared to the standard deviation of Z_{dr}, and the corresponding 95% confidence interval was estimated to be ±0.015 with a mean offset of -0.1 dB.

4: Rainfall rates and rain accumulations

The algorithms for rainfall estimation were based on scattering simulations using the 1-minute DSDs. The flowchart is very similar to that given in the appendix of Bringi et al. (2009) for C-band, except for the equations, which have been adapted for S-band. The following three estimators have been used: (i) the Z_h-R best-fit, (ii) the R-K_{dp} best-fit, and (iii) a combination of (i) and (ii) as well as the R(Z_h, Z_{dr}) best-fit. The synthetic or the composite algorithm uses R(Z_h), R(K_{dp}), or R(Z_h, Z_{dr}), depending on various threshold conditions, given in the flowchart in Fig. 6 which also summarizes the threshold conditions where each of the rain-rate equations [Eqs. (1)–(3)] are used. The thresholds for K_{dp} and Z_{dr} were based on considering the standard deviations of these measureables by using FIR range-filtered data in homogeneous (uniform reflectivity) regions of rain.

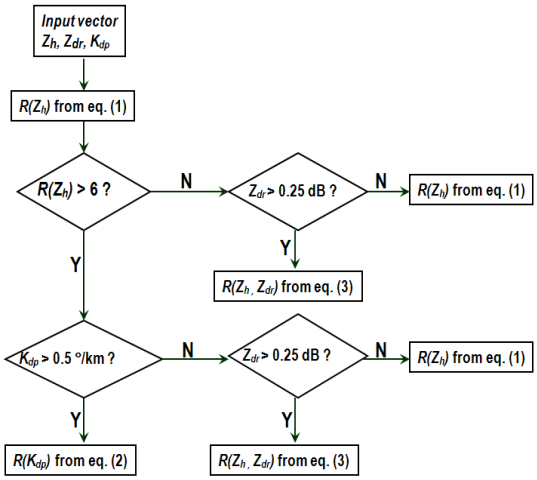

$$R(Z_h) = 0.0176 \left| Z_{h\_linear}^{0.6589} \right| \quad \text{..... (1)}$$

$$R(K_{dp}) = 34.3 \left| K_{dp}^{0.757} \right| \quad \text{..... (2)}$$

$$R(Z_h, Z_{dr}) = 0.0142 \frac{\left| Z_{h\_linear}^{0.77} \right|}{\left| Z_{dr\_linear}^{1.67} \right|} \quad \text{..... (3)}$$

Figure 6: Block diagram illustrating the composite algorithm for rain-rate estimation, together with the various values of applied thresholds.

Fig. 7a shows the rainfall rates derived from the NPOL data compared with those determined from the 1-minute DSDs from

the six 2DVD units. The calibration offsets for NPOL's Z_h and Z_{dr} have been included in the comparisons. The agreement is very good for all six cases, throughout the four-hour period. Fig 7b shows the corresponding rain accumulations, and once again, we see good agreement. The negligible bias in rain accumulation indicates that the calibration offset been estimated accurately, and furthermore, our composite algorithm derived from the 2DVD data has low parameterization error.

Fig. 8a and 8b show another event which occurred on 24 April 2011, just prior to the start of the MC3E campaign. This was a rapidly evolving multi-cell rain event (with large drops), reaching rainfall rates of over 50 mm/h in some cases and nearly 100 mm/h in one case (over SN36). Fig 8a is therefore plotted on a log scale, to depict the excellent agreement over a large (dynamic) range of rainfall rates estimated from the NPOL radar and the six 2DVD data.

The rain accumulations in Fig. 8b also show good agreement between the NPOL data based estimates and the six 2DVD data-based measurements. However, the variability of rainfall across the disdrometer array is also evident, for example, at the SN25 location the total rain accumulation for the 2-hour period was around 2 mm whereas at the SN36 location (nearly 10 km away) the corresponding accumulation exceeded 15 mm. The rain accumulation map for this event is given in Fig. 9 which clearly highlights large variations within a few km that arose due to the convective nature of the storm and the direction in which it moved. The locations of the six 2DVD instruments are also marked in the figure.

5. Summary

The external calibration offsets for radar reflectivity and differential reflectivity for NPOL radar during the MC3E campaign were determined by comparing the radar data extracted over the disdrometer sites with those determined from scattering simulations using the 2DVD data. Time series comparisons show excellent agreement for all six sites, and a technique was developed to determine the offsets quantitatively from the comparisons. The differences in time-matched reflectivity between NPOL data and the six 2DVD units were used to derive a PDF for $25 < Z < 35$ dBZ. The number of samples available was 610. It was found that the PDF of ΔZ (and ΔZ_{dr}) could be represented by a Gaussian distribution. From the standard deviation of the fitted curve, the 95% confidence interval for the estimated Z_h calibration offset was estimated to be -0.8 ± 0.12 dB. The corresponding confidence interval for Z_{dr} offset was -0.1 ± 0.015 dB.

The radar data were then used to determine the rain rates over the six 2DVD sites and compared with those derived from the 2DVD measurements. Once again, excellent agreement was obtained for all six sites, both in terms of rainfall rates and accumulations. Two events have been considered, including one rapidly evolving multi-cell rain event (with large drops) on 24 April 2011 which had rainfall rates ranging from 0.1 mm/h to nearly 100 mm/h. The good agreement found in the rainfall rates, and more importantly, rain accumulations, indicates the method used here provides an accurate estimate of radar calibration offsets.

(a)

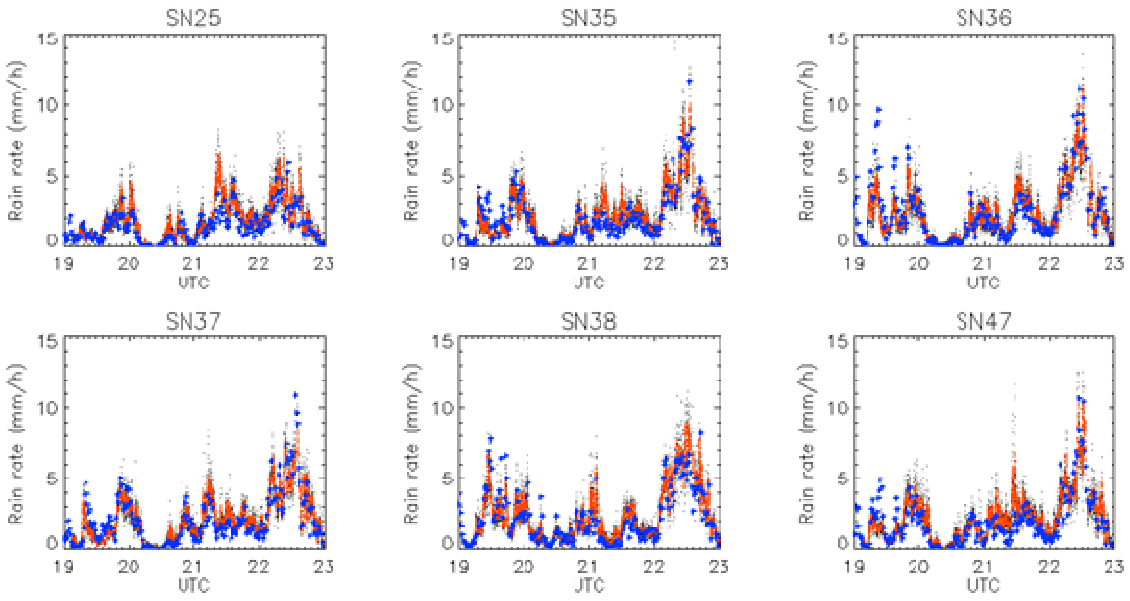

(b)

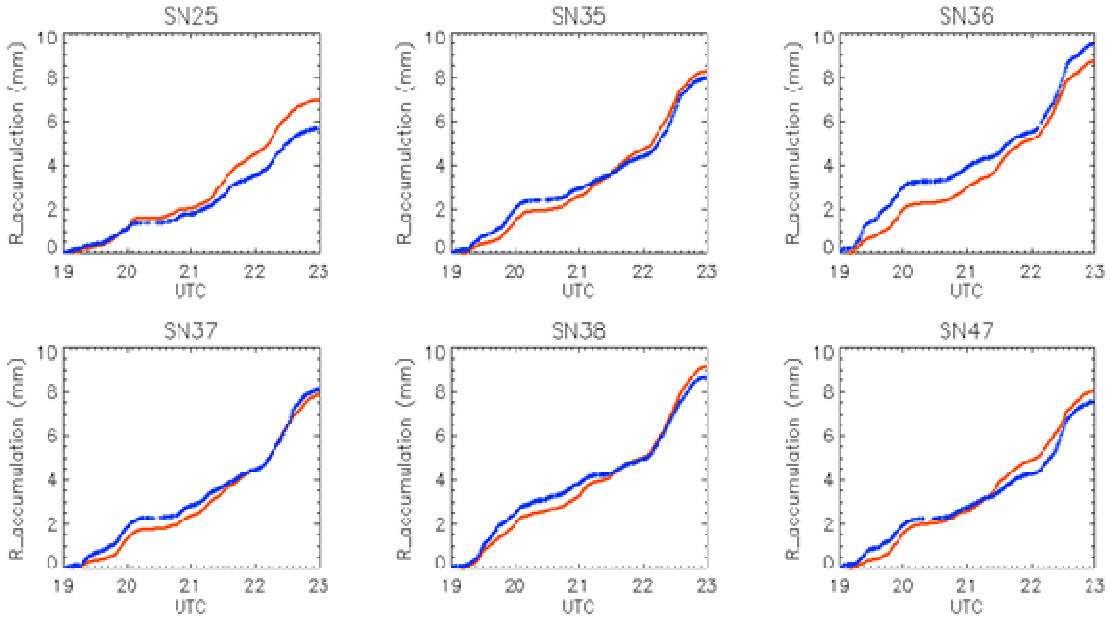

Figure 7. Rainfall (a) rate and (b) accumulation, for 11 May 2011 from NPOL radar (red) and the six 2DVD instruments (blue).

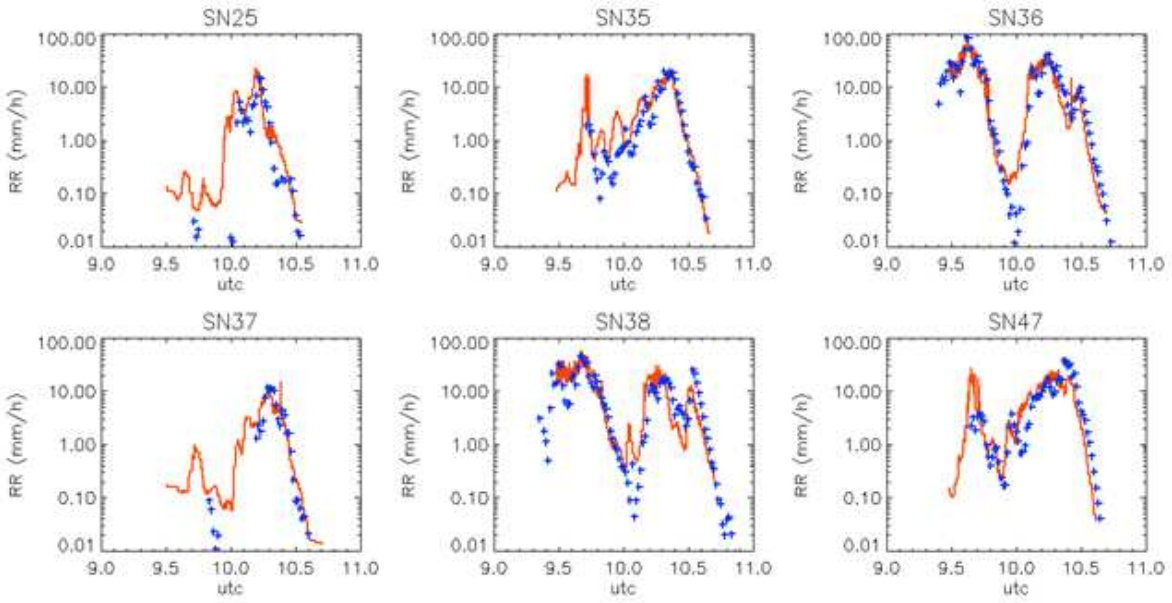

Figure 8a. Same as Figure 7a (NPOL-red; 2dvd-blue) except for a multi-cell storm on 24 April 2011 and rainfall rate in a) is plotted on a log scale using a different Z-R relationship in (1):

$$R(Z_h) = 0.0229\left(\mathrm{Z_{h\_linear}}^{0.6425}\right)$$

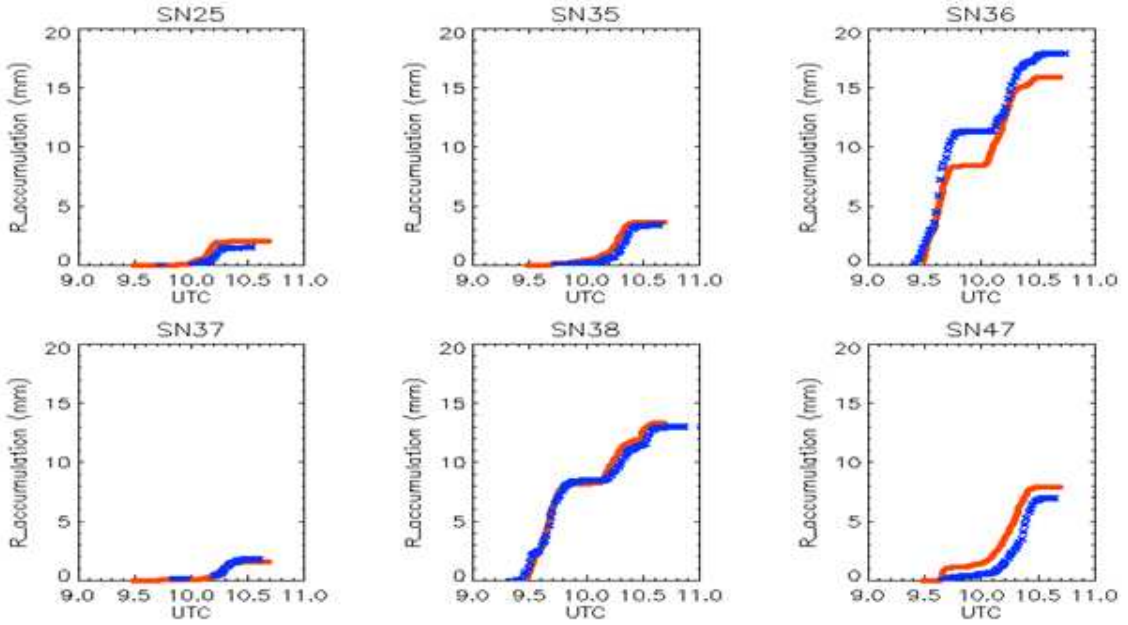

Fig. 8b: Comparisons of rain accumulations corresponding to Fig. 8a.

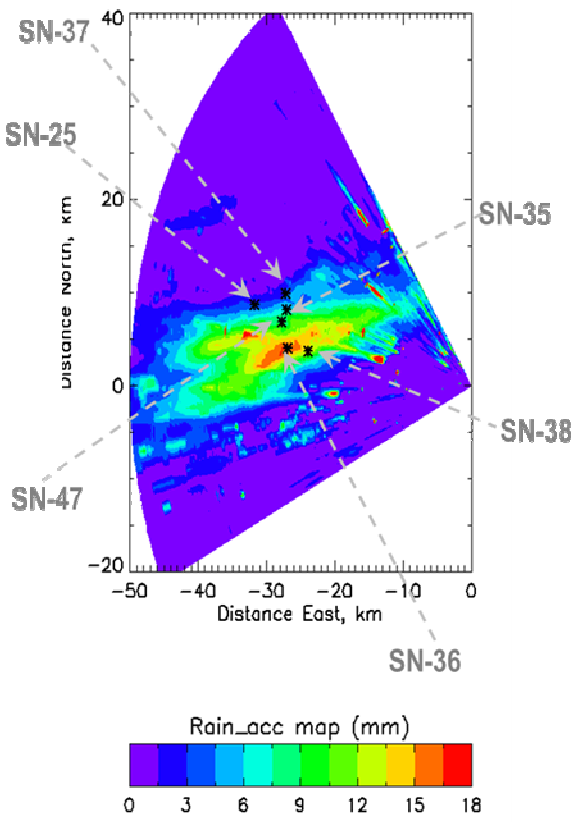

Fig. 9: Rain accumulation map for 24 April 2011, 09:30 – 10:42 UTC. The six 2DVD instruments are also marked.

Acknowledgments

We would like to thank the NPOL radar scientists and technicians as well as the disdrometer field technicians during MC3E for collecting the data used in this study. We would also like to thank Ramesh Kakar of the NASA Precipitation Measurement Mission and Arthur Hou and Mathew Schwaller of the NASA GPM program offices for providing funding for this study.

References

Aydin, K., T. A. Seliga, V. Balaji, 1986: Remote Sensing of Hail with a Dual Linear Polarization Radar. J. Climate Appl. Meteor., 25, 1475–1484.

Bringi V N, Seliga T A, Aydin K. Hail detection with a differential reflectivity[J]. Science, 1984,225:1 145-1 157.

Bringi, V. N., M. Thurai, K. Nakagawa, G. J. Huang, T. Kobayashi, A. Adachi, H. Hanado, and S. Sekizawa, 2006: Rainfall estimation from C-band polarimetric radar in Okinawa, Japan: Comparisons with 2D-video disdrometer and 400 MHz wind profiler. J.Meteor. Soc. Japan, 84, 705–724.

Bringi, V. N., C. R. Williams, M. Thurai, and P. T. May, 2009: Using dual-polarized radar and dual-frequency profiler for DSD characterization: A case study from Darwin, Australia. J. Atmos. Oceanic Technol., 26, 2107–2122.

Bringi, V.N., L. Tolstoy, M. Thurai and W. A. Petersen, 2013: Estimation of spatial correlation of rain drop size distribution parameters and rain rates using NASA's S-band polarimetric radar and 2D video disdrometer network: Two case studies from MC3E, Paper 240, 36th Radar Meteorology conference, (this conference), Breckenridge, CO, September 16 - 20, 2013.

Cavalli R., 1998: Operational experience with the new generation of Swiss radars'. Pp. 159–164 in COST-75 Advanced Weather Radar Systems—International Seminar, Locarno. European Commission, rue de la Loi 200, B-1049 Brussels, Belgium

Ciach, G. J., and W. F. Krajewski, 1999: On the estimation of radar rainfall error variance. Adv. Water Resour., 22, 585–595.

Darlington, T., M. Kitchen, J. Sugier, and J. de Rohan-Truba, 2003: Automated real-time monitoring of radar sensitivity and antenna pointing accuracy. 31st Conference on Radar Meteorology, AMS, 538–541.

Goddard, J., J. Tan, and M. Thurai, 1994: Technique for calibration of meteorological radars using differential phase. Electron. Lett., 30, 166–167.

Habib, E., and W. F. Krajewski, 2002: Uncertainty analysis of the TRMM ground-validation radar-rainfall products: Application to the TEFLUN-B field campaign. J. Appl. Meteor., 41, 558–572.

Hall, M. P. M., J. W. F. Goddard and S. M. Cherry, 1984, Identification of hydrometeors and other targets by dual-polarization radar, Radio Science, 19(1), 132–140.

Huang, G-J., V. N. Bringi, V. N., and M. Thurai, 2008: Orientation angle distributions of drops after an 80-m fall using a 2D video disdrometer, J. of Atmos. and Ocean. Tech., 25, 1717-1723.

Hubbert, J. and V. N. Bringi, 1995: An Iterative Filtering Technique for the Analysis of Copolar Differential Phase and Dual-Frequency Radar Measurements, J. Atmos. Ocean Tech., 12, 643-648.

Petersen W., and Jensen, M., 2012: The NASA-GPM and DOE-ARM Midlatitude Continental Convective Clouds Experiment (MC3E), The Earth Observer, Volume 24, Issue 1, January - February 2012, pp. 12-18.

Ryzhkov, A. V., S. E. Giangrande, and T. J. Schuur, 2005: Rainfall Estimation with a Polarimetric Prototype of WSR-88D. Journal of Applied Meteorol., 44, 502-515.

Thurai, M., G-J. Huang, V. N. Bringi, W. L. Randeu, and M. Schönhuber, 2007: Drop Shapes, Model Comparisons, and Calculations of Polarimetric Radar Parameters in Rain, Journal of Atmospheric and Oceanic Technology, 24, 1019-1032.

Thurai, M., V. N. Bringi, and W. A. Petersen, 2009: Rain microstructure retrievals using 2-D video disdrometer and C-band polarimetric radar. Adv. Geosci., 20, 13–18.

Thurai, M., V. N. Bringi, L. D. Carey, P. Gatlin, E. Schultz, W. A. Petersen, 2012: Estimating the Accuracy of Polarimetric Radar–Based Retrievals of Drop-Size Distribution Parameters and Rain Rate: An Application of Error Variance Separation Using Radar-Derived Spatial Correlations. J. Hydrometeor, 13, 1066–1079.